Assessment of Thrombotic Risk following Transcatheter Mitral Valve Replacement

Samuel J. Hill, Alistair Young, Ronak Rajani, Adelaide De Vecchi
School of Biomedical Engineering and Imaging Sciences
King's College London, United Kingdom

Abstract

Computational Fluid Dynamics (CFD) simulation is used to identify areas within the left ventricle following transcatheter mitral valve replacement that present haemodynamic conditions known to promote thrombus formation. The methodology is applied to two patients who required different devices, with two variations in deployment height for each subject. Blood residence time, Lagrangian particle tracking, wall shear stress and oscillatory shear index provide insight into ventricle haemodynamics and can be used to identify regions of potential device-induced thrombosis.

1. Introduction

Mitral Regurgitation (MR) is the flow of blood from the left ventricle (LV) upstream into the left atrium (LA) due to inadequate closure of the mitral valve and is one of the most common form of valvular heart disease. This currently the most prevalent cardiac disease in the United States with 2-2.5 million cases, estimated to grow to 5 million by 2030 [1]. Treatment options include repairing or replacing the native valve, with replacement commonly performed after failed repair. In frail and older patients, who are contraindicated for open-chest surgery, this is performed percutaneously via transcatheter mitral valve replacement (TMVR).

Early experiences of TMVR have shown great promise. However, local blood flow perturbations near the valve frame can lead to abnormal wall shear stress (WSS) on the device and high blood residence time (BRT) in the LV – all predisposing factors to the onset of valvular thrombosis, alongside common patient-specific risk factors such as LV dysfunction or atrial fibrillation [2]. As a result, oral anticoagulation is now recommended indefinitely following TMVR, although there is a lack of consensus as to the optimal duration of treatment and which patients require it [3,4]. This choice must be balanced against risks of bleeding in the post-procedural period, which are particularly relevant in a patient population at high surgical risk, and the fact that a mandate for long-term anticoagulation for all TMVR patients is likely to restrict more widespread clinical uptake. This context highlights the need for mechanistic studies to understand whether we can identify which patients have adverse blood residence profiles and should remain on long-term anticoagulation.

Flow-based metrics for the assessment of thrombotic risk like WSS and BRT are hard to measure in-vivo. We have thus developed a workflow for personalised CFD models of the LV with an implanted TMVR device, which are able to quantify non-invasively the postprocedural ventricular haemodynamics. Once validated in-vivo, these models have the potential to enhance risk assessment for valvular thrombosis and support personalisation of anticoagulation therapies.

2. Methods

The 3D finite-volume CFD models are based upon procedural imaging data and involves the manual segmentation of the LV blood pool to create a patient specific mesh. The mesh is then subjected to wall motion tracking throughout the cardiac cycle using Eidolon [5]. The implanted device is modelled via Computer Aided Design (CAD) and embedded within the mesh prior to simulation. CFD simulations are performed with the appropriate choice of physics solver parameters and boundary conditions using the STARCCM+ package (Siemens PLM). Lastly, the solution data are processed to extract metrics of interest such as WSS and Oscillatory Shear Index (OSI) on the device frame, BRT within the LV and Lagrangian particle tracking to identify areas with propensity to promote thrombus formation.

2.1. Patients

Two patients with severe MR were modelled for this study. The first (Case 1) was male, 61 years old and admitted after reporting dyspnoea and shortness of breath with an ejection fraction of 38%. The second (Case 2) was female, had an ejection fraction of 60% and a calcified mitral valve annulus with calcification extended to the leaflets. In both cases preprocedural multi-phase contrast-enhanced, gated CT datasets were acquired alongside 2D and Doppler echocardiography.

2.2. Image Processing

The end systolic frame of the CT images was segmented

using the software package MITKWorkbench [6]. Given the high sensitivity of flow parameters to the anatomy of the LV basal region, the angulation of the aorto-mitral junction, the septal bulge and the shape and area of the aortic and mitral valve were manually measured from the CT data and used to correct the segmentations. The surface was smoothed to obtain a regular surface mesh, from which a volumetric mesh with polyhedral cells was obtained.

Wall motion tracking was performed using an algorithm based on temporally sparse free-form deformation [5]. The wall motion was quantified as a vector field of displacements and applied to the vertices of the surface mesh, specific to the patient, for each CT frame throughout the cardiac cycle. Measurements were taken again at each time interval to validate the motion tracking against image derived measurements.

2.3. Device Modelling

CAD models of two commercial devices were generated based on the published manufacturers' specifications and embedded in the native MV in the LV mesh. Both devices rely on radial force for anchoring and have circular inner stents. The first device comprises of a conformable outer stent, a flexible brim to aid imaging during implantation and subsequent tissue in-growth, and a circular inner stent housing a tri-leaflet bovine pericardium valve. The size of the inner stent for Case 1 was 27mm.

The second valve was also a circular tri-leaflet device with bovine pericardial tissue and achieved sealing by means of an outer skirt. In Case 2 this device was modelled as a cylinder of inner diameter 23mm. Two deployment heights representing a more ventricular and more atrial deployment were modelled. The ventricular deployment model was chosen as extending deeper into the ventricle (60% of the total frame height inside the LV, 40% inside the LA), whereas in the atrial deployment the proportion was reversed (40% inside the LV, 60% inside the LA).

2.4. Simulation Set-up

The 3D incompressible Navier-Stokes equations were solved using a segregated flow solver with constant blood density ρ = 1060 Kg/m^3 and viscosity set to μ = 3.5 × 10^{-3} $Pa\,s$. The boundary conditions for the endocardium were derived from the wall motion tracked from the CT to prescribe nodal displacements in an incremental manner at each time-step. A mass flow boundary condition was prescribed for the mitral and aortic valves, based on the volume change within the ventricle at each time step. The time-step set as 0.0005s and a mesh independence study indicated a density of approximately 1.3 million cells are required for adequate convergence. Two cardiac cycles were simulated for both patients.

Key metrics for identifying thrombus formation include BRT inside the LV, WSS and OSI. A passive scalar and Lagrangian particle tracking were used to measure BRT within the LV. For the time-averaged magnitude of WSS (TAWSS) a field-mean monitor approximates the temporal integration of the equation below.

$$TAWSS = \frac{1}{T}\int_{t-T}^{t} |WSS|dt \qquad (1)$$

Where,

$|WSS|$ is the instantaneous WSS magnitude
t is the instantaneous time
T is the period of the cardiac cycle.

OSI quantifies the oscillatory nature of the WSS vectors and is calculated from Eq. (1).

$$OSI = 0.5 \times \left(1 - \frac{\left|\frac{1}{T}\int_{t-T}^{t} WSSdt\right|}{\frac{1}{T}\int_{t-T}^{t}|WSS|dt}\right) \qquad (2)$$

3. Results

Results for the ventricular and atrial deployments for the two cases are summarised in Tables 1 and 2 below.

Table 1 - Case 1 results for ventricular and atrial deployment

	Ventricular	Atrial
WSS Surface-averaged Max (Pa)	2.58	2.97
WSS Max (Pa)	47.68	34.41
Max BRT (s)	1.45	1.52
Location of Max BRT	Apex	Apex

Table 2 - Case 2 results for ventricular and atrial deployment

	Ventricular	Atrial
WSS Surface-averaged Max (Pa)	17.19	7.96
WSS Max (Pa)	99.87	89.75
Max BRT (s)	0.99	1.00
Location of Max BRT	Anterior Wall	Apex

3.1. Blood Residence Time

For Case 1, for both deployment heights the maximum BRT occurred in the apical region (Figure 1A, B). Although the apical BRT was similar, the shift from atrial to ventricular deployment led to a sharp increase of BRT in the region between the anterior wall and the valve frame (mean local BRT 0.90s and 1.11s for atrial and ventricular deployment respectively), as shown in Figure 1A, B.

In Case 2, the ventricular deployment showed higher BRT near the anterior wall and inside the valve frame (Figure 1C), in the atrial deployment however blood with high residence time accumulated in the apical region similar to Case 1 (Figure 1D).

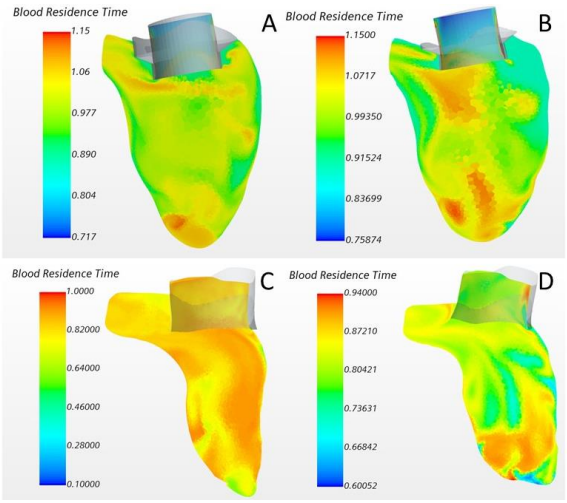

Figure 1 - Isocontours of blood residence time of (A, C) ventricular and (B, D) Atrial deployments during peak systole

3.2. Wall Shear Stress

In both patients the maximum WSS is greater in the ventricular deployments than their atrial counterparts (Table 1 and 2). The WSS magnitude on the valve surface showed that the highest region of stress in all cases is on the posterior side of the prosthetic valve near the left ventricular outflow tract (Figure 2). The surface-averaged WSS was comparable in both deployments for Case 1, but in Case 2 a marked increase was observed in the ventricular deployment, where it increased from 6.5Pa to 17.2Pa during systole (Figure 3). This is consistent with the higher velocity of the blood flow being ejected in this patient (which reached a maximum value of 2.55m/s at peak systole, as opposed to 1.33m/s in Case 1) (Figure 2A, C) and the larger proportion of the left ventricular outflow tract obstructed by the device frame. A small area of flow recirculation is also observed in the upper outflow tract in the case during systole, unlike in Case 1 (Figure 2A, C).

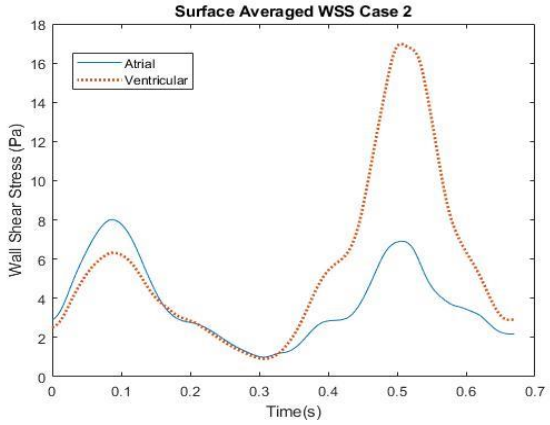

Figure 1 - Surface averaged WSS Case 2 in the atrial and ventricular deployment over the cardiac cycle

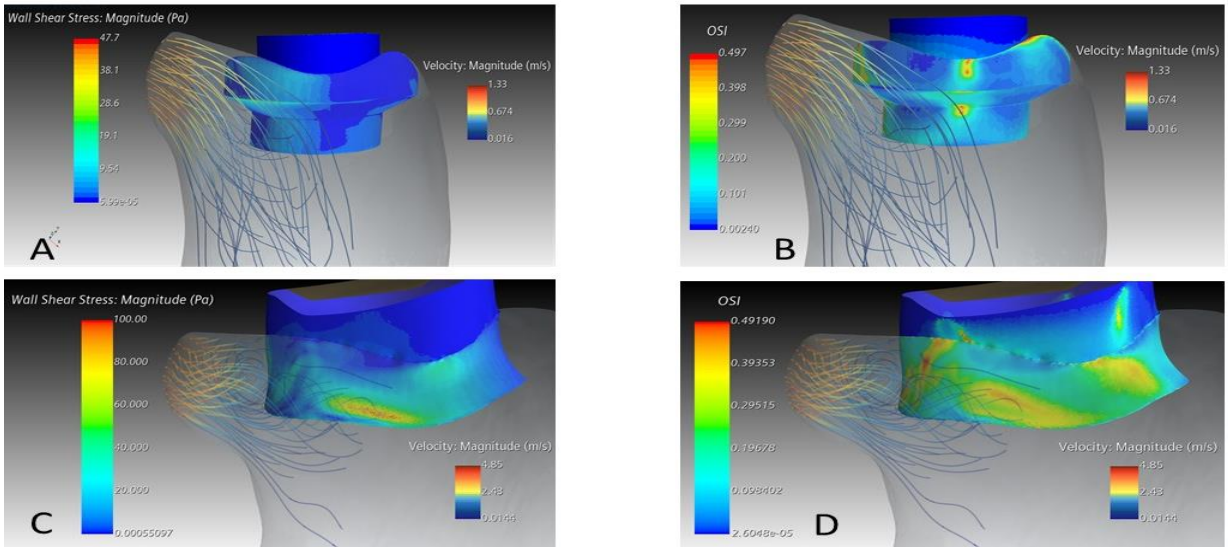

Figure 2 - Isocontours of WSS (A, C) and OSI (B, D) for the ventricular deployments of Case 1 and 2 during peak systole

3.2. Oscillatory Shear Index

The maximum OSI reached in both cases was 0.49, and can be seen at all stages of the simulation due to the oscillatory nature of the flow (Figure 2). In Case 1 pockets of low OSI (<0.1) formed on the sides of the valve frame near the left ventricular outflow tract, especially near the oblique section below the fixation ring, surrounded by localised sharp increases of OSI (>0.4), as shown in Figure 2 B. In Case 2 large areas of high OSI formed on the whole surface of the device frame (Figure 2 D).

4. Discussion

At a macroscopic level, thrombus formation mechanisms are driven by the interplay of flow parameters like blood residence time, WSS, and OSI. From a mechanistic standpoint, high WSS can lead to blood damage and abnormal platelet activation, which is a well-known phenomenon in ventricular assist devices [7]. Once platelets are activated, regions of blood stasis (or high BRT) can facilitate accumulation and adhesion mechanisms, leading to thrombus initiation. Areas of high BRT in the LV are characterised by low blood velocity, resulting in low WSS, and flow recirculation patterns, which are associated with high OSI. Such low oscillatory wall shear stresses are known to affect endothelial cell activation and promote thrombus growth in vessels, although their role in device-induced thrombosis in the LV is less clear and under researched [8]. Pro-thrombogenic factors such as high BRT, high OSI, low WSS, and contact between blood and a foreign material are present in the narrow region between the anterior ventricular wall and the device frame as observed in Case 1 with ventricular deployment. This scenario may present ideal conditions for thrombus formation. The extent of these areas is highly influenced by the anatomical shape of the ventricle and the device model and the positioning with a shift from ventricular to atrial deployment leading to an 18% reduction in BRT in this region for Case 1. Moreover, partial obstruction in the left ventricular outflow tract, as observed in Case 2 with ventricular deployment, and high ejection fraction result in high surface-averaged WSS on the device (with maximum value approximately 3 times higher than in Case 1) and blood recirculation in the upper outflow tract. In Case 2 the ventricular deployment also leads to a proportion of the flow being trapped inside the valve frame during ejection, which also contributes to generate low oscillating WSS and high BRT inside the prosthesis.

These results show how the multi-factorial relationship between the patient-specific anatomy and hemodynamics, and the device shape and deployment can contribute to shaping pro-thrombogenic conditions. While direct clinical evidence on thrombotic risk following TMVR is still limited, patient-specific and device-specific CFD models enable an in-depth mechanistic understanding of risk factors and their relations, as well as provide a robust evaluation of the predictive power of macroscopic flow metrics. Once fully validated, these models could be used in conjunction with clinical imaging to identify areas of high thrombotic risk for patients considered for TMVR, thus supporting a shift towards personalisation of antithrombotic strategies.

Acknowledgments

This research was supported by the EPSRC [EP/R513064/1].

References

[1] Vaquerizo B, Theriault-Lauzier P, Piazza N. Percutaneous Transcatheter Mitral Valve Replacement: Patient-specific Three-dimensional Computer-based Heart Model and Prototyping. Rev Esp Cardiol, 2015, 68(12):1165-73. doi: 10.1016/j.rec.2015.08.005.

[2] Pagnesi M, Moroni F, Beneduce A, Giannini F, Colombo A, Weisz G, Latib A. Thrombotic Risk and Antithrombotic Strategies After Transcatheter Mitral Valve Replacement. JACC Cardiovasc Interv. 2019, 9;12(23):2388-2401. doi: 10.1016/j.jcin.2019.07.055.

[3] Nishimura RA, Otto CM, Bonow RO, Carabello BA, Erwin JP 3rd, Fleisher LA, Jneid H, Mack MJ, McLeod CJ, O'Gara PT, Rigolin VH, Sundt TM 3rd, Thompson A. AHA/ACC Focused Update of the 2014 AHA/ACC Guideline for the Management of Patients With Valvular Heart Disease: A Report of the American College of Cardiology/American Heart Association Task Force on Clinical Practice Guidelines. Circulation, 2017, 20;135(25):e1159-e1195. doi: 10.1161/CIR.000000000 503.

[4] Egbe AC, Pislaru SV, Pellikka PA, Poterucha JT, Schaff HV, Maleszewski JJ, Connolly HM. Bioprosthetic Valve Thrombosis Versus Structural Failure: Clinical and Echocardiographic Predictors. J Am Coll Cardiol. 2015, 1;66(21):2285-2294. doi: 10.1016/j.jacc.2015.09.022.

[5] E. Kerfoot et al., “Eidolon: Visualization and computational framework for multi-modal biomedical data analysis,” in Lecture Notes in Computer Science, 2016, vol. 9805 LNCS, pp. 425–437.

[6] A. Fetzer, S. Zelzer, T. Schroeder, H.-P. Meinzer, and M. Nolden, An interactive 3D segmentation for the Medical Imaging Interaction Toolkit (MITK). MICCAI Proc, 2014, doi: 10.13140/2.1.4169.6326

[7] Fraser, K. H., Zhang, T., Taskin, M. E., Griffith, B. P., and Wu, Z. J. A Quantitative Comparison of Mechanical Blood Damage Parameters in Rotary Ventricular Assist Devices: Shear Stress, Exposure Time and Hemolysis Index. ASME. J Biomech Eng, 2012,134(8): 081002

[8] Di Achille P., Tellides G., Figueroa C. A. and Humphrey J. D. A haemodynamic predictor of intraluminal thrombus formation in abdominal aortic aneurysms. Proc. R. Soc. A, 2014, 470. doi:10.1098/rspa.2014.0163

Address for correspondence:
Samuel Joseph Hill
School of Biomedical Engineering and Imaging Sciences, King’s College London, St Thomas’ Hospital, London, SE1 7EH, UK
Email: Samuel.hill@kcl.ac.uk